Scientific Research Publishing

World Journal of Engineering and Technology, 2026, 14(2), 389-404
https://www.scirp.org/journal/wjet
ISSN Online: 2331-4249
ISSN Print: 2331-4222

A Material Removal Prediction Framework for Ball EEM Polishing in Precision Lens Manufacturing

Tyler Young[1], Jacob Guymon[1,2], Mark Pankow[1,3], Gracious Ngaile[1]

[1]Department of Mechanical and Aerospace Engineering, North Carolina State University, Raleigh, NC, USA
[2]KLA Corporation, Milpitas, CA, USA
[3]National Reconnaissance Office, Chantilly, VA, USA
Email: gngaile@ncsu.edu

How to cite this paper: Young, T., Guymon, J., Pankow, M. and Ngaile, G. (2026) A Material Removal Prediction Framework for Ball EEM Polishing in Precision Lens Manufacturing. *World Journal of Engineering and Technology*, **14**, 389-404.
https://doi.org/10.4236/wjet.2026.142022

Received: February 6, 2026
Accepted: April 4, 2026
Published: April 7, 2026

Abstract

Lens surface parameters are critical to optical system performance and require increasingly stringent precision due to rising performance demands and continued technological miniaturization. Although machining processes such as diamond turning can produce lenses with high form accuracy, they are not free from surface defects. These defects are typically addressed through post-processing techniques such as polishing; however, depending on defect size and the selected removal process, polishing can become a complex and iterative task. This complexity can be mitigated through the application of machine learning algorithms to predict material removal behavior. This paper presents the development of a material removal prediction framework for ball elastic emission machining (EEM) polishing of lens surfaces, incorporating machine learning tools to improve process predictability and efficiency. The resulting model accepts surface characteristics and process parameters as inputs and predicts the final surface parameters following polishing. The model's root mean square error (RMSE) is approximately 0.1 μm. Surface parameters achieved using the removal strategy on which this model is based include a peak-to-valley (PV) value of 0.2841 μm and a root mean square (RMS) roughness of 0.032 μm.

Keywords

Optics, Machine Learning, Metrology, Modeling, Polishing, Toolpathing

1. Introduction

The continuous advancement of modern technology has driven the simultaneous

demands for component miniaturization and increased manufacturing precision. Optical technologies, in particular, have experienced rapid progress with recent developments in micro-lens arrays, advanced coatings, and high-performance optical systems [1]-[3]. These applications require extremely high levels of surface accuracy, which are typically achieved through advanced machining processes. Lens fabrication at the precision scale commonly involves grinding, milling, or diamond turning. Among these, diamond turning has gained significant attention in precision optics due to its ability to produce nanometer-scale surface finishes, depending on the workpiece material, tool geometry, and machine parameters [4] [5]. In parallel, emerging fabrication techniques such as focused ion beam (FIB) lithography have demonstrated the capability to reliably generate nano-architectures for advanced optical components [6]. While these methods meet the stringent performance requirements of precision optics, they often do so at the expense of increased manufacturing time and cost.

To address these limitations, mold-based fabrication has emerged as a cost-effective alternative for large-scale lens production. Molds enable consistent replication of lens geometry and surface finish at reduced cost; however, surface defects present in the mold are directly transferred to each replicated lens. Consequently, post-processing methods such as polishing are essential for correcting mold surface errors and improving both surface form and finish. This work focuses on surface correction through elastic emission machining (EEM), a non-contact polishing technique suitable for ultra-precision applications. EEM is a material removal process that utilizes an accelerated slurry to chemically interact with the workpiece surface, inducing controlled atomic-scale removal. Material removal may be achieved by directing slurry flow using nozzles or by accelerating slurry across the workpiece surface through mechanical motion. Regardless of the delivery mechanism, the removal process is governed by a complex interaction of factors, including workpiece material properties, process parameters, slurry chemistry, and fluid dynamics [7] [8]. Due to this complexity, experimentally deriving accurate removal models is both time-consuming and resource-intensive, particularly when multiple materials and process conditions are involved.

Several studies have investigated material removal modeling and optimization from different perspectives. Zhao *et al.* developed a removal profile model for non-contact shear thickening polishing (NCSTP), accounting for tool movement angle, tool rotation, machining gap, and flow field characteristics [9]. Their model integrated shear-thickening fluid simulations with microscopic abrasive removal mechanisms, achieving a maximum average error of 4.45% while reducing surface roughness (Ra) from 465.77 nm to 41.55 nm. Wang *et al.* examined the removal rate of graphene oxide-enhanced slurry during polishing of single-crystal diamond, studying the influence of rotation speed, particle size, and grain hardness through femtosecond laser-etched contour measurements [10]. Zhao *et al.* proposed a weak magnetization-enhanced stress-rheological polishing (WM ESRP) removal model based on non-Newtonian fluid dynamics and microscopic contact

mechanics, reporting a maximum deviation of 5.7% between theoretical and experimental results [11]. Zhang *et al.* introduced specialized polishing tools to improve surface quality while maintaining form accuracy, developing damping and profile damping tools suitable for removal depths ranging from tens to hundreds of micrometers [12]. Their approach incorporated a shape evolution model accounting for finite slip on microstructured surfaces. Ma *et al.* conducted multiple investigations into EEM material removal, including a three-dimensional model simulating slurry-wheel interaction and atomic removal energy to predict removal profiles [7]. In a related study, Ma *et al.* introduced active gap control to regulate fluid film thickness, improving surface RMS from 0.553 nm to 0.085 nm through hydrodynamic lubrication analysis [8]. Additional modeling efforts include femtosecond laser polishing optimization of reaction-bonded silicon carbide [13], abrasive rotating jet polishing for inner surfaces [14], laser polishing parameter optimization using response surface methodology [15], and electrorheological polishing profile modeling based on contact pressure and relative velocity [16].

With recent shifts toward data-driven manufacturing, machine learning has gained increasing interest as a tool for optimizing material removal and part fabrication. Machine learning models can leverage process-relevant sensor data to predict surface parameters and improve polishing outcomes [17]. Randomness in material removal processes has also been explored to enhance surface prediction accuracy and overall surface quality [18]. Zhelyeznyakov *et al.* optimized metalenses using a physics-informed neural network coupled with an overlapping boundary method, achieving a 53% improvement in maximum intensity while maintaining a reasonable manufacturing time of 15 minutes [19]. Prabuwono *et al.* proposed a robotic polishing system that classifies surface defects using neural networks, with force and rotation time as outputs, noting limitations in visual-based defect classification but demonstrating applicability depending on accuracy requirements [20]. Zhou *et al.* introduced a lens mold compensation approach using a random forest algorithm, improving form error by 63.5% based on RMSE, coefficient of determination (R^2), and out-of-bag (OOB) metrics [21].

Building on these advances, the present study focuses on expanding a previously established ball EEM material removal model for Stavax steel lens molds [22]. Unlike full-surface polishing approaches, the model targets localized material removal for lens profile correction and is characterized accordingly. The methodology integrates experimental removal data with MATLAB-based scripts for defect identification, toolpath projection, and removal prediction using fitted approximations. This work aims to enhance the predictability and efficiency of targeted EEM polishing by combining physical process understanding with data-driven modeling techniques, thereby providing a practical framework for precision lens manufacturing.

2. Methodology and Data Collection Setup

Elastic emission machining (EEM) is a corrective polishing process capable of

achieving atomic-scale material removal through chemically mediated interactions between slurry particles and the workpiece surface. In EEM, a particle-laden slurry is accelerated across the surface, where bonding and subsequent detachment of surface atoms result in controlled material removal. Several approaches exist for slurry acceleration, including nozzle-based systems, hydrodynamic disks, and rotating-tool configurations. This work focuses on a rotating ball-type EEM system, which provides localized and controllable removal suitable for precision lens correction. In the rotating EEM configuration, a compliant spherical tool mounted on a rotating spindle accelerates the slurry through surface contact. The elastic compliance of the sphere allows controlled pressure distribution within the contact zone while reducing the risk of surface damage. A schematic diagram of the ball-type EEM polishing principle, and the lens correction experimental setup are shown in Figure 1.

Material removal in EEM is governed by several interacting parameters, including applied normal load, dwell time, spindle speed, tool geometry and compliance, and slurry particle characteristics. Understanding and controlling these parameters is essential for predictable and repeatable material removal. The slurry used in this work is a mixture of 70% water and 30% particles, with the particles being 0.05 μm diameter alumina microspheres.

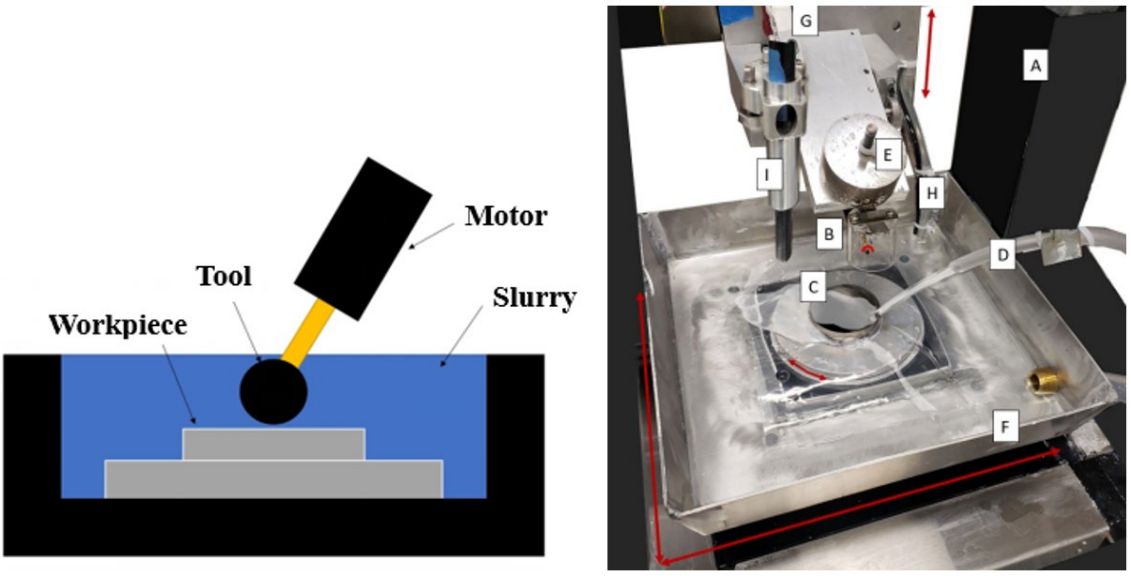

(a) (b)

Figure 1. (a) Schematic Illustration of Ball-Type Elastic Emission Machining (EEM) Polishing; (b) Targeted Lens Correction Experimental Setup. A, Griffin 4-axis precision stage (red arrows show axis motion direction). B, Tool/Ball (red arrow shows tool rotation direction). C, Workpiece on rotational stage. D, Slurry delivery system. E, Preload. F, Slurry recovery tray. G, Tool load cell. H, Workpiece cleaning system with water and air. I, Non-contact confocal aberration probe.

The experimental data used for material removal prediction were collected using a four-axis ultra-precision motion system consisting of an XY translation

stage, a Z-axis stage, and a rotational B-axis. The XY stage provides 150 mm of travel in each direction, while the Z-axis offers 100 mm of vertical travel. The linear axes have sub-micron resolution and repeatability on the order of 1 μm, while the rotational B-axis provides angular resolution on the order of 1 arc-second. The workpiece is mounted to the B-axis using a kinematic coupling mechanism, ensuring repeatable positioning and alignment across multiple polishing and measurement cycles. The EEM polishing tool consists of a rubber spherical polishing head mounted on a spindle and oriented at an angle of 30˚ relative to the workpiece surface. This orientation was selected to balance tool clearance and contact patch symmetry while remaining compatible with the system geometry. The spherical tool has a diameter of 3.18 mm and a Shore A hardness between 70 and 80, providing sufficient elastic compliance for controlled polishing. A load cell integrated into the system enables closed-loop force control, allowing the Z-axis position to be adjusted in real time to maintain a constant polishing load during dwell-based operations.

On-machine metrology is a critical element of the methodology, enabling direct correlation between tool motion and resulting material removal. A chromatic confocal aberration (CA) probe is integrated into the system to provide non-contact, high-resolution surface measurements without removing the workpiece (**Figue 1(b)**-I). The probe is mounted as an extension of the Z-axis tooling and provides a vertical resolution of 20 nm over a measurement range of 300 μm, with a working distance of 4.5 mm and a spot diameter of approximately 4 μm. This configuration enables in situ surface mapping before and after polishing, forming the basis for the material removal prediction framework.

3. Data Processing and Material Removal Prediction Framework

3.1. Surface Measurement Processing

All surface measurement and processing routines were implemented in MATLAB. On-machine chromatic confocal probe data, including XYZ position and height measurements, were imported from the motion controller and converted to physical units using calibrated scaling factors. The measured surface data were spatially aligned with the tool coordinate system to ensure consistency between measurement and polishing coordinates.

Following alignment, the data were filtered to improve spatial uniformity and reduce noise. A minimum point spacing criterion was enforced to prevent excessive clustering, while tilt correction and statistical outlier removal were applied to eliminate measurement artifacts. After filtering, surface form metrics, including peak-to-valley (PV) and root-mean-square (RMS) error, were computed and used as baseline indicators for subsequent correction.

3.2. Identification of Removal Locations

An ideal lens surface was defined using a specified nominal curvature and com-

pared to the measured surface to generate a residual map. Here, the residual is defined as the pointwise height difference between the measured surface and the nominal surface, while the residual map represents the spatial distribution of these differences across the lens surface. Positive residual values correspond to regions of excess material that require removal, whereas negative values indicate regions below the nominal surface.

The residual map served as the primary basis for identifying localized surface features requiring correction. Removal locations were selected by applying a residual threshold, such that only regions exceeding a specified residual magnitude were targeted for material removal. This threshold was progressively reduced as surface quality improved through successive polishing iterations, enabling increasingly fine corrective actions.

Each selected removal location corresponds to a dwell point, defined as a discrete surface position at which the polishing tool is positioned and held stationary to induce localized material removal. To control removal density and prevent localized over-polishing, a point-skipping strategy was implemented, limiting the number of adjacent dwell points within a given region. The resulting set of dwell points typically ranged from several hundred to approximately one thousand points, depending on dwell time, surface area, and removal magnitude.

3.3. Dwell-Based Removal Modeling

Material removal was modeled using experimentally measured dwell profiles, which describe the spatial distribution of material removed during a single dwell event under constant loading conditions. Dwell tests were conducted at a load of 20 g for multiple dwell times, where dwell time is defined as the duration for which the polishing tool remains stationary at a dwell point. Experimental results confirmed a near-linear relationship between dwell time and removal volume within the operating range of this study.

To isolate steady-state material removal behavior, a zero-second dwell test was performed to quantify and subtract the initial contact contribution. The measured dwell profiles were then approximated using surface polynomial fits, enabling removal prediction at arbitrary surface locations.

During simulation, the polynomial removal function was applied to all surface points within the effective dwell radius, generating a simulated dwell removal field for each dwell point. The dwell center was shifted to account for tool inclination and elastic deformation effects. Dwell time at each removal location was scaled relative to the local residual magnitude, allowing increased material removal at surface peaks while preventing excessive removal in lower regions.

3.4. Validation of Removal Prediction

Predicted surface profiles were generated by superimposing the simulated dwell removals onto the measured surface. **Figure 2** presents a comparison between the experimentally measured surface profile and the predicted material removal for a

representative polishing iteration (33rd pass). Prior to correction, the measured lens surface exhibited a peak-to-valley (PV) error of 0.8009 μm and a root mean square (RMS) error of 0.1209 μm, indicating localized surface deviations requiring targeted material removal. Using the process parameters applied during this pass, the proposed removal prediction framework generated a projected surface profile with a predicted PV of 0.7249 μm and an RMS of 0.1439 μm. There is notable improvement in the PV of the surface while RMS is worsened by 23 nm. This is emblematic of the issues with the size of the contact area for the removal process when applying it to the point-based removal approach implemented in the material removal prediction program. The program targets high points, which more often yield greater improvements in the PV of the system, while, depending on the location of the high point relative to other surface features, some low points can be gouged as a result, yielding non-ideal changes to the RMS. This issue is resolved through the use of the program in an iterative removal process. As the surface is refined and the PV decreases the removal also becomes more uniform due to the scaling dwell method used.

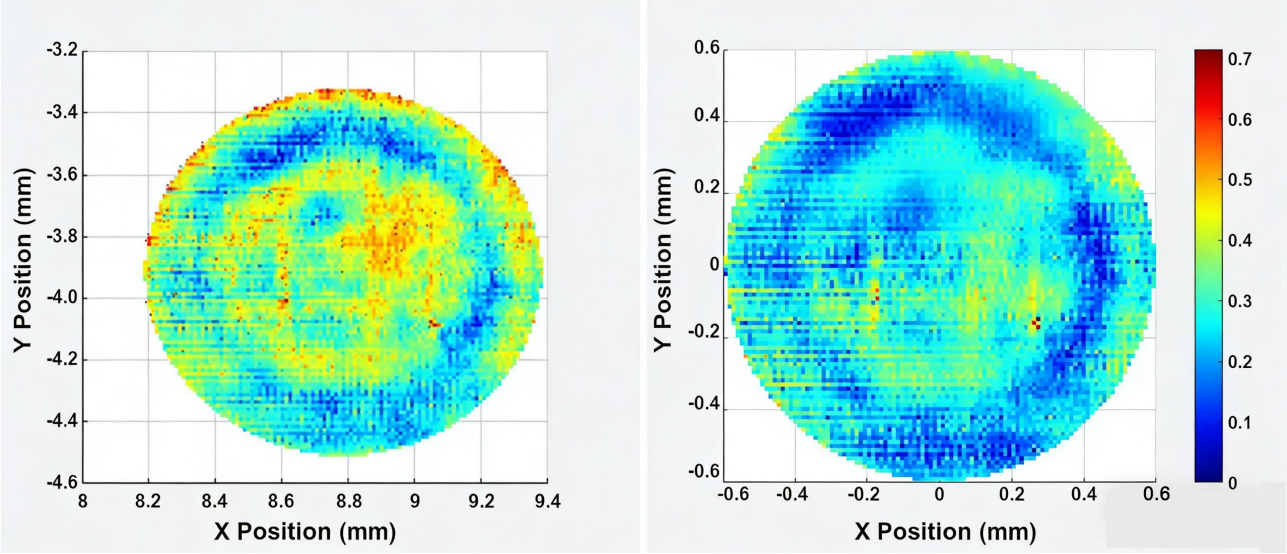

Figure 2. Comparison between experimentally measured surface and predicted material removal for the 33rd polishing pass. The measured surface (left) and model-predicted removal profile (right) demonstrate close agreement in removal trends and spatial distribution.

The spatial distribution of the predicted removal closely matches the experimentally measured surface features, demonstrating that the model captures both the magnitude and location of material removal with sub-micron fidelity. Although minor differences in RMS are observed, the overall agreement confirms that the framework reliably predicts removal trends for localized EEM polishing operations. These results validate the effectiveness of the dwell-based removal model as a tool for guiding corrective polishing and reducing form error in precision lens manufacturing.

Figure 3 illustrates the evolution of surface form error as the proposed material

removal prediction framework is applied iteratively over successive polishing passes. Starting from the initial surface condition, each correction step was guided by the predicted removal profile, enabling targeted reduction of localized form errors rather than uniform material removal. As the number of passes increased, both peak-to-valley (PV) and root mean square (RMS) surface errors decreased monotonically, demonstrating stable convergence of the correction strategy. After the final correction pass, the lens surface achieved a PV of 0.2841 μm and an RMS of 0.032 μm, representing a substantial improvement relative to the pre-correction condition. The consistent reduction in surface error across iterations confirms that the prediction model not only captures single-pass removal behavior but also remains reliable when embedded within a multi-pass corrective polishing workflow. These results highlight the effectiveness of the proposed framework for deterministic surface correction in ball EEM polishing, enabling predictable convergence toward high-precision optical surface requirements.

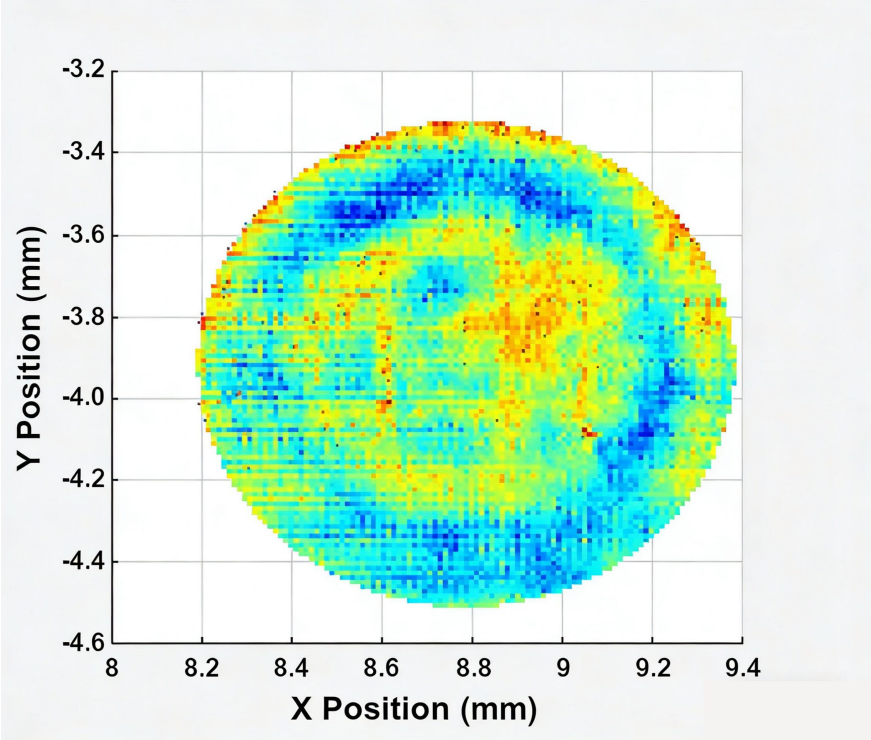

Figure 3. Final lens residual following several iterations of prediction toolpaths, PV = 0.2841 um and RMS = 0.0320.

4. Machine Learning-Based Optimization of EEM Material Removal

The deterministic material removal prediction framework described in Section 3 enables accurate simulation of surface evolution for a prescribed toolpath and set of polishing parameters. However, identifying optimal polishing parameters, such as dwell scaling, residual thresholds, and correction density, through repeated physics-based simulations alone can be time-consuming. To address this limita-

tion, a data-driven machine learning (ML) approach was introduced to rapidly predict post-polishing surface outcomes and guide parameter selection prior to detailed simulation.

In this work, the ML model functions as a surrogate screening tool, meaning it rapidly evaluates candidate polishing parameter combinations and estimates expected surface outcomes. Unfavorable parameter sets can therefore be excluded before computationally intensive deterministic simulations are performed. Importantly, the ML model complements, rather than replaces, the physics-based removal framework.

4.1. Dataset Generation and Feature Selection

The machine learning model was trained using data generated from the validated deterministic removal simulation described in Section 3. Each data instance corresponds to a single polishing iteration, defined here as one complete corrective polishing pass applied to the surface using a specified set of toolpath and process parameters. Although the dataset was generated through simulation, the embedded removal behavior is governed by experimentally validated dwell profiles and physically calibrated removal mechanics. As such, the simulated data remain physically representative of the EEM process.

The selected input features were chosen to capture the dominant factors governing material removal behavior and can be grouped into three categories: 1)Initial surface state descriptors, including peak-to-valley (PV) and root mean square (RMS) error prior to polishing; 2) Toolpath and correction parameters, such as residual bounds, dwell scaling factors, and number of dwell points; and 3) Process conditions, including applied load and nominal dwell duration. The output variables were the predicted post-polishing PV and RMS values. The parameters for the model training were selected based on a range relative to the typical level used for polishing. The residual bound varied from 1.2 to 4 μm, consisting of 0.1 μm steps from 1.2 to 2.6 μm and 0.2 μm steps from 2.6 to 4 μm. Dwell time for the model was set from 1 to 3 seconds in steps of 0.5 seconds. It should be noted that while it is not a controllable parameter in the prediction process, the number of removal points from each simulation was also stored and factored in as a model parameter.

The sampling method used for this simulated data collection process was a full factorial parameter sweep to provide the most insight into the possible material removal for each measurement. Simulated cases that resulted in over-correction or non-physical removal behavior were explicitly accounted for and labeled. This allowed the model to learn practical operating limits and penalize infeasible parameter combinations. These types of removal were identified through comparison of the new profile to the ideal lens form. If a point in the profile goes beyond the depth of the point in the lens based on a set tolerance, in this case 2% of the residual magnitude, the run is flagged as over-correction. This was incorporated into the model as an additional predictor in the form of a true/false parameter to identify whether the parameters would yield an invalid surface. It is important to distinguish between two uses of the term *residual* in this manuscript: In Section

3, *residual* refers to surface form deviation relative to the nominal lens geometry. In this section, *regression residual* refers to the difference between the ML-predicted and true post-polishing surface metrics (PV or RMS).

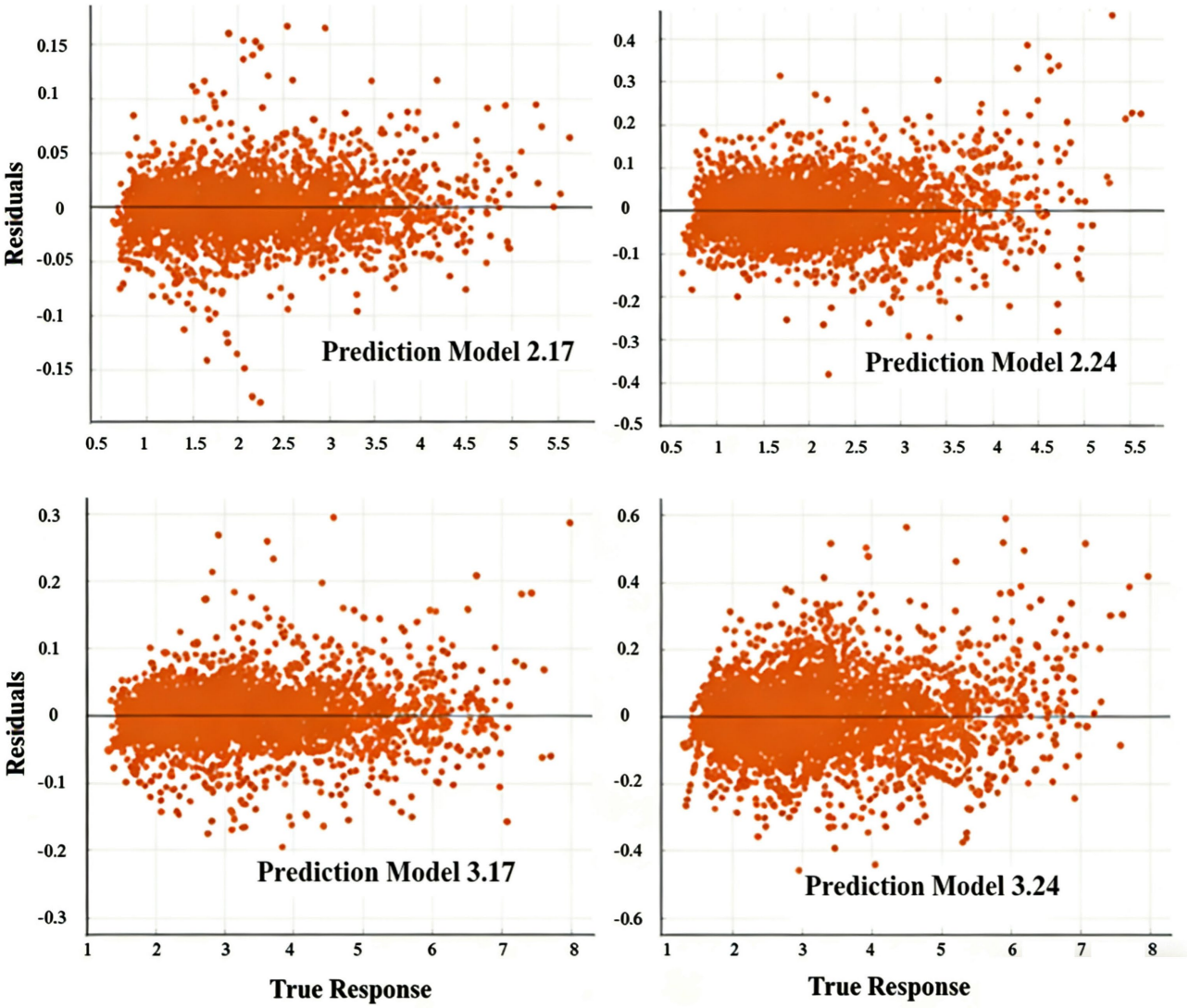

Figure 4. Residual comparison of regression models used for predicting post-polishing surface metrics. Residuals represent the difference between predicted and true PV or RMS values. Gaussian Process Regression (GPR) exhibits the lowest residual dispersion and minimal bias, indicating superior predictive performance relative to alternative models.

4.2. Regression Model Selection and Performance Evaluation

Multiple regression techniques were evaluated, including neural networks and support vector machines. Among these, Gaussian Process Regression (GPR) demonstrated superior performance in capturing smooth, nonlinear trends while maintaining physically consistent predictions. GPR is particularly well-suited for this application because it interpolates sparse data while enforcing smoothness consistent with the continuous nature of material removal. The model was trained to predict post-polishing PV and RMS values given the selected input parameters.

Figure 4 compares the regression residual distributions for the evaluated models. Here, residual dispersion refers to the spread of prediction error across the dataset, while systematic bias indicates consistent over- or under-prediction relative to true values. The GPR model exhibits the lowest dispersion and minimal bias compared to the alternative models, indicating improved generalization across the simulated dataset. Based on this performance, GPR was selected as the primary machine learning model for subsequent optimization and integration.

4.3. Response Surface Analysis and Parameter Trade-Offs

To better understand the influence of polishing parameters on predicted surface quality, response surface visualizations were generated using the trained GPR model. The response surfaces shown in Figure 5 represent ML-predicted trends across the parameter space, rather than direct experimental measurements. Figure 5 illustrates representative response surfaces showing the relationship between dwell scaling, residual bounds, and predicted post-polishing RMS and PV values. Here, dwell scaling refers to a proportional factor used to adjust dwell time magnitude based on local surface residuals; residual bounds define the upper and lower surface deviation limits used to select correction locations; and the dwell threshold specifies the minimum residual magnitude required for a dwell point to be applied. These surfaces reveal clear trade-offs between correction aggressiveness and achievable surface quality.

These surfaces reveal clear trade-offs between correction aggressiveness and achievable surface quality. Here, correction aggressiveness refers to the combined effect of dwell scaling, residual thresholds, and dwell point density, which collectively determine the magnitude and spatial concentration of material removal. Regions of diminishing returns and potential over-correction are visible in the response surfaces.

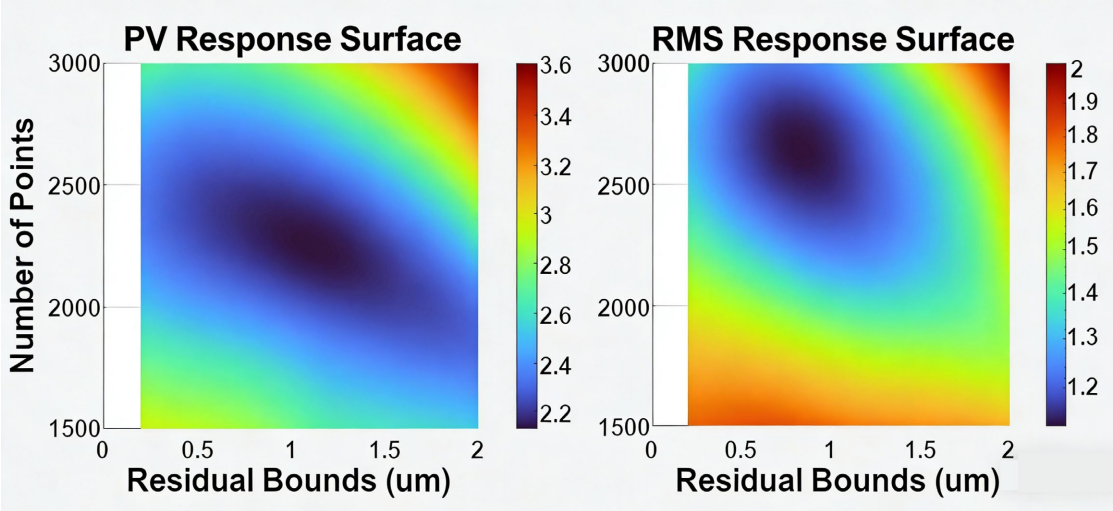

Figure 5. Representative GPR-predicted response surfaces showing the influence of dwell scaling and residual bounds on post-polishing PV and RMS values. The surfaces illustrate trade-offs between correction aggressiveness and achievable surface quality.

These visualizations provide physical insight into the parameter space, enabling identification of operating regions that balance efficient material removal with surface stability. Importantly, these predicted trends remain consistent with deterministic simulation results and experimental observations, reinforcing the physical relevance of the data-driven model.

4.4. Integration with Deterministic Simulation

The response surfaces presented in Figure 5 provide insight into how individual polishing parameters influence post-polishing surface quality metrics, specifically peak-to-valley (PV) and root mean square (RMS) error. However, parameter combinations that minimize PV do not necessarily minimize RMS, and vice versa. As a result, selecting polishing parameters based on a single response surface can lead to suboptimal trade-offs in overall surface quality.

To identify parameter combinations that simultaneously yield acceptable PV and RMS values, the feasible regions extracted independently from the PV and RMS response surfaces were intersected. This intersection represents the subset of polishing parameters that satisfy performance criteria for both surface metrics. Figure 6 illustrates this intersection in parameter space, highlighting combinations that balance form correction and surface smoothness. The Gaussian Process Regression (GPR) model was used to evaluate the response surfaces and define feasibility criteria based on predicted post-polishing surface metrics. Parameter combinations outside this feasible intersection were excluded, as they were predicted to either produce insufficient correction or lead to over-aggressive removal and potential surface degradation. The resulting feasible region therefore represents a constrained optimization space rather than a single global optimum.

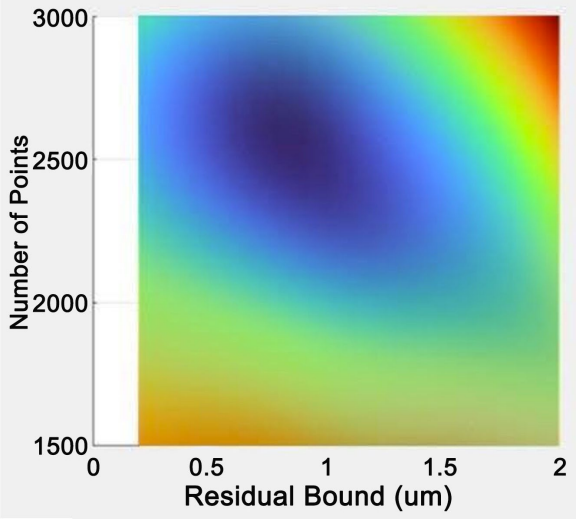

Figure 6. Intersection of feasible polishing parameter regions derived from the PV and RMS response surfaces shown in Figure 5. The highlighted overlap represents parameter combinations predicted by the Gaussian Process Regression (GPR) model to simultaneously satisfy PV and RMS performance criteria and is used to guide subsequent deterministic removal simulations.

The parameter combinations identified within this intersected region were subsequently passed to the deterministic dwell-based removal framework described in Section 3. These parameter combinations can be run through the machine learning model much faster and with significantly reduced computational cost than the original framework. Output of the projected PV and RMS from the model can be weighted based on the needs of the project and current magnitude of the surface to identify the ideal combination of PV and RMS improvement for each removal step on a case-by-case basis. Detailed simulations were then used to verify physical realizability, generate toolpaths, and predict surface evolution under experimentally validated removal physics. This hybrid workflow allows the machine learning model to rapidly narrow the parameter search space, while the deterministic simulation ensures accuracy, stability, and physical interpretability of the polishing process.

The integration of deterministic dwell-based modeling with data-driven parameter screening establishes a unified framework for predictive and efficient EEM optimization. The following section summarizes the primary technical contributions and implications of this hybrid methodology.

5. Conclusions

This study presents a hybrid physics-based and data-driven framework for predictive material removal and optimization in ball elastic emission machining (EEM) applied to precision lens mold correction. Experimental dwell tests were performed under different loading conditions to determine removal profiles, which were then integrated into an iterative polishing strategy to enhance the form and finish of a Stavax lens mold. After surface refinement, the polishing program was converted into an automated framework to generate simulated datasets for training machine learning models. The combination of machine learning with traditional EEM parameters allowed for predictive control of material removal and surface quality, achieving sub-micrometer precision in the polishing process. The following conclusions can be drawn:

- A deterministic dwell-based removal model was developed and experimentally validated, demonstrating the ability to predict localized material removal with sub-micron accuracy for targeted EEM polishing operations.
- Iterative application of the removal framework enabled stable convergence of surface form error, reducing peak-to-valley (PV) and root mean square (RMS) values to 0.2841 μm and 0.032 μm, respectively, confirming the robustness of the correction strategy.
- A Gaussian Process Regression (GPR) model was successfully trained using simulation-generated data constrained by experimentally validated removal physics. The model accurately predicts post-polishing surface metrics and identifies non-physical overshoot conditions.
- Integration of the machine learning model with the deterministic simulation framework enables rapid screening of polishing parameters, significantly re-

ducing reliance on manual tuning and trial-and-error approaches.

- The proposed hybrid methodology preserves the physical interpretability of EEM removal mechanisms while introducing a scalable and efficient optimization strategy suitable for precision optical manufacturing.

While the present study focuses on Stavax steel lens molds and a specific ball-type EEM configuration, the framework is readily extensible to other materials, tool geometries, and corrective polishing applications with appropriate retraining and calibration. Future work will explore direct incorporation of experimental feedback into the learning process and extension of the framework to freeform optical surfaces.

Conflicts of Interest

The authors declare no conflicts of interest regarding the publication of this paper.

References

[1] Enoch, J.M. (2009) The Fascinating Early History of Optics! Archaeological Optics 2009: Our Knowledge of the Early History of Lenses, Mirrors, and Artificial Eyes! *Proceedings of the Society of Photo-Optical Instrumentation Engineers*, **7428**. https://doi.org/10.1117/12.828453

[2] Sreekanth, K.V., Prabhathan, P., Chaturvedi, A., Lekina, Y., Han, S., Zexiang, S., *et al.* (2022) Wide-Angle Tunable Critical Coupling in Nanophotonic Optical Coatings with Low-Loss Phase Change Material. *Small*, **18**, Article 2202005. https://doi.org/10.1002/smll.202202005

[3] Yuan, W., Li, L., Lee, W. and Chan, C. (2018) Fabrication of Microlens Array and Its Application: A Review. *Chinese Journal of Mechanical Engineering*, **31**, Article No. 16. https://doi.org/10.1186/s10033-018-0204-y

[4] Abou-El-Hossein, K., Kadirgama, K., Kadernani, M., Chikamhi, P. and Oyekunle, F.A. (2023) Surface Roughness in Ultra-High Precision Diamond Turning of Silicone Hydrogel Contact Lenses. *Materials Science Forum*, **1099**, 21-25. https://doi.org/10.4028/p-u4cahs

[5] He, C.L., Zhang, J.G., Ren, C.Z., Wang, S.Q. and Cao, Z.M. (2022) Characteristics of Cutting Force and Surface Finish in Diamond Turning of Polycrystalline Copper Achieved by Friction Stir Processing (FSP). *Journal of Materials Processing Technology*, **301**, Article 117451. https://doi.org/10.1016/j.jmatprotec.2021.117451

[6] Keskinbora, K., Grévent, C., Hirscher, M., Weigand, M. and Schütz, G. (2015) Single-step 3D Nanofabrication of Kinoform Optics via Gray-Scale Focused Ion Beam Lithography for Efficient X-Ray Focusing. *Advanced Optical Materials*, **3**, 792-800. https://doi.org/10.1002/adom.201400411

[7] Ma, W., Li, J. and Hou, X. (2023) Rolling Model Analysis of Material Removal in Elastic Emission Machining. *International Journal of Mechanical Sciences*, **258**, Article 108572. https://doi.org/10.1016/j.ijmecsci.2023.108572

[8] Ma, W., Li, J. and Hou, X. (2024) Profile Prediction and Analysis in Active Controlled Elastic Emission Machining. *International Journal of Mechanical Sciences*, **275**, Article 109274. https://doi.org/10.1016/j.ijmecsci.2024.109274

[9] Zhao, J., Wang, W., Qiu, X., Wang, Z. and Fan, C. (2025) Material Removal Profile

Model Simulations and Experiments on the Non-Contact Shear Thickening Polishing of K9 Glass. *Journal of Manufacturing Processes*, **134**, 435-451. https://doi.org/10.1016/j.jmapro.2024.12.055

[10] Wang, Z., Zhao, Y., Yao, J., Yu, T., Qu, S. and Zhao, J. (2024) The Investigation of Graphene Oxide-Enhanced Hybrid Slurry Preparation and Its Polishing Characteristic on CVD Single Crystal Diamond. *Materials*, **17**, Article 6053. https://doi.org/10.3390/ma17246053

[11] Zhou, D., Li, X., Huang, X. and Ming, Y. (2023) Theoretical and Experimental Investigations on Material Removal Characteristics of Small-Diameter Aspherical Silicon Carbide Mould with Weak Magnetization-Enhanced Force-Rheological Polishing. *Tribology International*, **179**, Article 108106. https://doi.org/10.1016/j.triboint.2022.108106

[12] Zhang, P., Jing, Z., Goel, S., Hou, X., Wang, C., Cheung, C.F., *et al.* (2024) Theoretical and Experimental Investigations on Conformal Polishing of Microstructured Surfaces. *International Journal of Mechanical Sciences*, **268**, Article 109050. https://doi.org/10.1016/j.ijmecsci.2024.109050

[13] Yang, T., Liu, C., Chen, T., Shao, M., Jiang, C., Lu, C., *et al.* (2023) Parameter Optimization of RB-SIC Polishing by Femtosecond Laser. *Materials*, **16**, Article 1582. https://doi.org/10.3390/ma16041582

[14] Zhao, J., Ge, J., Khudoley, A. and Chen, H. (2024) Numerical and Experimental Investigation on the Material Removal Profile during Polishing of Inner Surfaces Using an Abrasive Rotating Jet. *Tribology International*, **191**, Article 109125. https://doi.org/10.1016/j.triboint.2023.109125

[15] Mushtaq, R.T., Wang, Y., Bao, C., Chen, X., Anwar, S., Sharma, S., *et al.* (2024) Multi-objective Optimization of Laser Polishing Parameters for Enhanced Mechanical Properties, Sustainability, and Surface Finish of 3D-Printed Industrial ABS Polymers Using Response Surface Methodology (RSM). *Journal of Materials Research and Technology*, **29**, 3168-3184. https://doi.org/10.1016/j.jmrt.2024.02.023

[16] Fan, C., Liu, K., Chen, Y., Xue, Y., Zhao, J. and Khudoley, A. (2022) A New Modelling Method of Material Removal Profile for Electrorheological Polishing with a Mini Annular Integrated Electrode. *Journal of Materials Processing Technology*, **305**, Article 117589. https://doi.org/10.1016/j.jmatprotec.2022.117589

[17] Schneckenburger, M., Höfler, S., Garcia, L., Almeida, R. and Börret, R. (2021) Material Removal Predictions in the Robot Glass Polishing Process Using Machine Learning. *SN Applied Sciences*, **4**, Article No. 33. https://doi.org/10.1007/s42452-021-04916-7

[18] Zhu, C., Gu, P., Wu, Y., Liu, D. and Wang, X. (2019) Surface Roughness Prediction Model of SiCp/Al Composite in Grinding. *International Journal of Mechanical Sciences*, **155**, 98-109. https://doi.org/10.1016/j.ijmecsci.2019.02.025

[19] Zhelyeznyakov, M., Fröch, J., Wirth-Singh, A., Noh, J., Rho, J., Brunton, S., *et al.* (2023) Large Area Optimization of Meta-Lens via Data-Free Machine Learning. *Communications Engineering*, **2**, Article No. 60. https://doi.org/10.1038/s44172-023-00107-x

[20] Prabuwono, A.S., Besari, A.R.A., Zamri, R., Md Palil, M.D. and Taufik, (2011) Surface Defects Classification Using Artificial Neural Networks in Vision Based Polishing Robot. In: Jeschke, S., Liu, H. and Schilberg, D., Eds., *Lecture Notes in Computer Science*, Springer, 599-608. https://doi.org/10.1007/978-3-642-25489-5_58

[21] Zhou, T., Gao, L., Yu, Q., Wang, G., Zhou, Z., Yan, T., *et al.* (2024) Machine Learning for Aspherical Lens Form Accuracy Improvement in Precision Molding of Infrared

Chalcogenide Glass. *Precision Engineering*, **90**, 156-163.
https://doi.org/10.1016/j.precisioneng.2024.08.007

[22] Guymon, J. (2023) Nanometer Level Surface Correction for Fine Optics. Ph.D. Thesis, North Carolina State University.
https://www.lib.ncsu.edu/resolver/1840.20/41136